COVER PAGE

1) What is the problem being addressed by the manuscript and why is it important to the Antennas & Propagation community? (limited to 100 words).

    a) Scan loss is a reduction in antenna gain as the steering angle increases. It is due to the element factor and array factor of a planar antenna. Scan loss affects the link budget in millimeter wave wireless communication systems, so needs to be mitigated in order to maximize the received signal power and hence the data rate.

2) What is the novelty of your work over the existing work? (limited to 100 words).

    a) The use of additional lens gain at wide scan angles in order to mitigate scan loss. Previous literature has considered the use of cascaded lenses in the boresight direction [14] [15] [16] [17], but not towards wide steering angles.

    b) The use of a cascaded zone plate triplet to provide additional lens gain at wide scan angles.

    c) Tilting the side lenses to align with the maximum steered angle. This maximises the projected area and thus the focusing directivity in that direction and reduces the scan loss.

    d) A novel method is proposed to calculate the special amplitude distributions when steering between the central and side lenses.

3) Provide up to three references, published or under review, (journal papers, conference papers, technical reports, etc.) done by the authors/coauthors that are closest to the present work. Upload them as supporting documents if they are under review or not available in the public domain. Enter "N.A." if it is not applicable.

    a) T. A. Hill and J. R. Kelly, "28 GHz Taylor feed network for sidelobe level reduction in 5G phased array antennas," *Microw. Opt. Tech. Lett.*, vol. 61, no. 1, pp. 37-43, Jan. 2019. This was attached to the original submission as a supporting document, and corresponds to reference [27].

    b) T. A. Hill, J. R. Kelly, M. Khalily, T. W. C. Brown, "Conformal Transmitarray for Scan Loss Mitigation with Thinned Reconfiguration," in *Proc. Eur. Conf. Antennas Propag. (EuCAP)*, Krakow, Poland, 2019. This is attached as a supporting document, and corresponds to reference [40].

4) Provide up to three references (journal papers, conference papers, technical reports, etc.) done by other authors that are most important to the present work. Enter "N.A." if it is not applicable.

    a) B. Schoenlinner, X. Wu, J. P. Ebling, G. V. Eleftheriades, and G. M. Rebeiz, "Wide-scan spherical-lens antennas for automotive radars," *IEEE Trans. Microw. Theory Tech.*, vol. 50, no. 9, pp. 2166-2175, 2002.

    b) J. Oh, G. Z. Hutcheson, F. Aryanfar, W. Hong, and Y. J. Lee, "Planar beam steerable lens antenna system using non-uniform feed method," *IEEE Antennas Propag. Soc. AP-S Int. Symp.*, pp. 651-652, 2014.

    c) A. Abbaspour-Tamijani, L. Zhang, and H. Pan, "Enhancing the directivity of phased array antennas using lens-arrays," *Prog. Electromagn. Res.*, vol. 29, pp. 41-64, February 2013.

Cascaded Fresnel Lens Antenna for Scan Loss Mitigation in Millimeter Wave Access Points

Timothy A. Hill, James R. Kelly *Member, IEEE*,

Mohsen Khalily *Senior Member, IEEE*, Tim W. C. Brown *Member, IEEE*

Abstract—Millimeter wave lens antennas will be essential for future wireless access. Conventionally, they increase the gain in the boresight direction only. In this paper, cascaded Fresnel zone plate lenses are combined with a phased array to increase the gain at wide steering angles of $\pm 52°$. The side lenses are tilted to align with the maximum steering angle, and cascaded to increase the focusing gain. The inner lenses increase the gain by 2.45 dB at boresight, and by 3.19 dB at the maximum steering angle. When the side lenses are repositioned, the simulated focusing gain increases to 4.69 dB. Asymmetric amplitude distributions are proposed to prevent the main lobe from splitting. An 8-element 7-lens prototype operating at 28 GHz achieved a gain from 12.96 dBi to 15.35 dBi with a bandwidth of at least 1.3 GHz for all measured beam directions. The maximum measured azimuthal beamwidth was 27°. A design procedure and a theoretical analysis of diffraction through the lenses are provided. By increasing the SNR, this beamforming antenna could improve the coverage of 3-sector 5G microcell base stations, and support gigabit wireless links for vehicular, rail, and satellite communications.

Index Terms—Lens antennas, dielectric antennas, beam steering, diffraction, phased arrays.

I. Introduction

ENHANCED mobile broadband will be required to support much higher data rates than previous generations of mobile technology. Within smart cities, this could enable applications such as ultra-high definition video streaming, remote healthcare, and vehicular connectivity. A wide bandwidth is available for future communications at millimeter wave frequencies. However, high path loss in this frequency band necessitates the use of directional antennas to satisfy the link budget [1]. Additionally, beam steering is needed to align the main lobe of the antenna with the user, maximizing the received signal power. Phased arrays enable continuous beam steering, increasing the minimum gain achieved within the steering range [2]. However, conventional phased array antennas suffer from impairments such as pointing misalignment

loss and scan loss [3]. These impairments degrade the signal-to-interference-and-noise ratio (SINR), and hence the quality of service experienced by the mobile users [1] [4]. Scan loss typically reduces the SINR by at least 3 dB at a 60° steering angle.

Simply increasing the transmitted power or the array size is not an effective solution to compensate for scan loss at millimeter wave frequencies. If the peak power is increased for wide steering, the power amplifier will operate at backoff for the boresight direction, reducing the system efficiency [1]. Similarly, the long feed lines in a large array incur high conductor losses, reducing the antenna efficiency [5]. This motivates the design of novel antennas with low scan loss.

Several electronically steered antennas, presented in the literature, have achieved scan loss mitigation. A metamaterial ground plane can be used to spread the element factor of a phased array, increasing the gain at wide steering angles (approaching end-fire) [6]. However, broadening the element factor reduces the boresight gain. Alternatively, a phase-shifting surface (PSS) lens fed by a phased array has been reported [7]. A boresight gain of 19 dBi was achieved, but the steering range was just $\pm 20°$.

At wide viewing angles, the projected area of a planar structure reduces [8]. This beamwidth broadening effect reduces the gain [9], contributing to scan loss. Conformal arrays can be used to alleviate this [10], but for a given direction, only a sub-set of the elements will be active in forming the beam. This reduces the achievable gain.

Quasi-optical methods can be used to increase antenna gain. A spherical lens illuminated by a set of 33 radiating elements virtually eliminated scan loss whilst providing high gain and low sidelobe level (SLL) [11]. However, the main beam could only be switched between discrete directions corresponding to the locations of the radiating elements. Also this approach requires the use of a single-pole multi-throw switch, which typically has a high insertion loss, thus significantly reducing the realized gain of the antenna [12]. In [13], a dielectric lens was mounted above a 60 GHz horn antenna to enhance the steering range. The lens was mechanically rotated on a lever to 50°, reducing the scan loss to 1.1 dB at 45°. However, mechanical steering limits the steering speed and reliability.

In this paper, we demonstrate how a phased array can be combined with lenses to counteract scan loss.

The substantive novelty presented in this paper is as follows:

1) The use of additional lens gain at wide scan angles in order to mitigate scan loss. Previous literature has considered the use of cascaded dielectric lenses in the

boresight direction [14] [15] [16] [17]. However, there is little, if any, existing literature on the use of additional lens gain at wide scan angles.

2) The use of a cascaded zone plate triplet to provide additional lens gain at wide scan angles. This prevents blockage of the central lens. To the authors' knowledge, this is the first cascaded zone plate triplet operating at millimeter wave frequencies.

3) Tilting the side lenses to align with the maximum steered angle. This maximises the projected area and thus the focusing directivity in that direction and reduces the scan loss.

By using phased arrays, the design avoids the need for a complex and costly switch matrix such as that used in [18]. When steering the beam to angles between the central and side lenses it is necessary to take additional steps to prevent beam splitting and to ensure that the width of the main beam remains approximately constant. This problem is unique and has not been encountered before in the literature. For this reason, we have developed a new form of asymmetric amplitude distribution which is applied to the phased array. Existing methods for calculating these distributions require iterative optimisation [19] [20]. We have developed a technique for calculating the required amplitude distributions in a single iteration.

The proposed design offers low scan loss across a moderately wide steering range, making it suitable for use within 5G small-cell access points. Hence, this millimeter wave beamforming antenna could be used to enhance user experience without increasing the transmitted power.

This paper is organized into six sections. Section II presents the operating principles of the novel antenna. In Section III, we detail a design procedure for the lenses. Section IV describes the prototype fabrication. Section V presents simulated and measured results, Section VI compares these with the state-of-the-art, and Section VII summarizes the key findings. Finally, a theoretical model of the diffraction through the lenses is presented in the Appendix.

II. OPERATING PRINCIPLES

Scan loss L_s is defined as the reduction in gain from the boresight gain $G(0)$ to the gain at the maximum scan angle $G(\theta_{0max})$ [21]. It significantly reduces the received signal power.

$$G(\theta_0) \propto \cos^{1.5}(\theta_0) \tag{1}$$

$$L_s(\text{dB}) = G(0)(\text{dBi}) - G(\theta_{0max})(\text{dBi}) \tag{2}$$

where $G(\theta_0)$ is the gain at scan angle θ_0 [2] [22].

A single Fresnel zone plate lens is a flat structure. Due to the beamwidth broadening problem, it is only able to provide maximum focusing gain to rays that pass through the lens at angles close to the normal. This corresponds to the boresight direction. The proposed antenna consists of several lenses, arranged on a circular arc (Fig. 1). The lenses in the proposed antenna align with a wider range of beam directions than
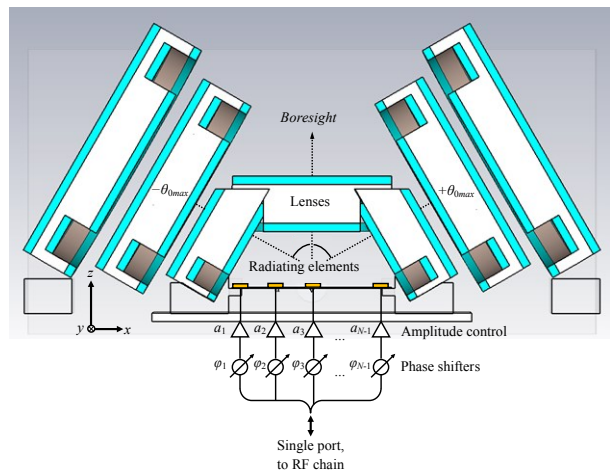

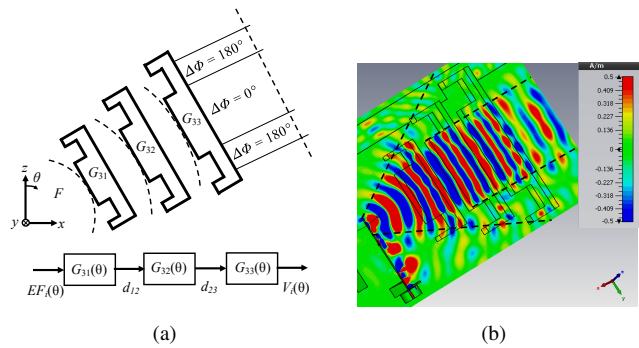Fig. 1. Cross-section through the antenna structure: lenses fed by a phased array.

Fig. 2. Operation of the cascaded lenses. (a) Block diagram showing successive diffractions. (b) H field magnitude showing beamwidth narrowing (gain increase). The feeding antenna is Taylor $\beta = 144°$.

would be the case for a single flat lens. The lenses are fed by a phased array antenna, which is steered from $-\theta_{0max}$ to $+\theta_{0max}$. This novel lens arrangement reduces beamwidth broadening by magnifying the projected area of the phased array. By maintaining an equal projected area in the direction of each steered beam, the proposed antenna can support wider steering angles, covering a base station sector from -60° to +60°. The aim of the design is similar to a wide angle lens in optics, but is implemented in a novel way at millimeter wave frequencies (quasi-optics). As the steering angle approaches the horizon, the apparent length of the array is increased when viewed through the lenses.

At wide steering angles, several lenses are cascaded on the same axis. The aim of this is to restore the gain at θ_{0max} to the value obtained at boresight and thus compensate for scan loss. The same lens shape is used throughout the design, which reduces the complexity.

The role of the lenses is to enhance the gain. The lenses repeatedly focus the wavefronts by successive diffractions through scaled concentric rings of phase shifts. These use the scaling property of the spatial Fourier transform (with a phase difference due to the wave propagating along the distance between lenses), to focus the beam [23] [16]. The benefit of this is that the whole structure can be analysed mathematically
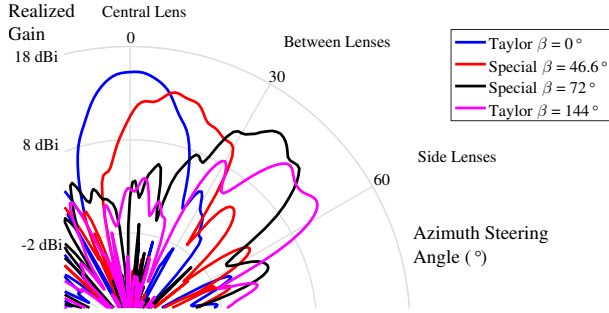
Fig. 3. Simulated azimuth radiation patterns, illustrating beam steering towards positive steering angles. The use of special amplitude distributions is demonstrated in the angular region between the central and side lenses.

by modelling the behavior of an individual lens.

In the enhanced design, the outer lens was repositioned further from the phased array source, as shown in Fig. 21 in Section V. In this case, the structure behaves as a microwave telescope, magnifying the object according to the ratio of the outer and middle lens focal lengths, F_3/F_2 [36]. Hence, the focusing gain is based on similar triangles, and the corresponding ratio of distances from the intermediate focal point. In this case, the image is inverted relative to the object (array source), because the rays cross at an intermediate focal point.

Instead of plano-convex lenses, zone plates are used, within the proposed antenna, to reduce the thickness. This simplifies manufacture, but reduces the focusing gain. To prevent blockage between adjacent lenses, the lens diameters are minimized by using a small number of zones. This enables several lenses to fit around the phased array. The zone radii, which determine the focal length, are scaled to achieve different focal lengths within the cascaded (compound) zone plate triplet.

If a single lens was used to obtain the required gain at the maximum scan angle, then that lens would need to have a very large diameter. This would cause blockage, as explained above. Furthermore, it would be difficult to design a single lens which could focus a beam to all of the angles within the scan angle range of the phased array.

Fig. 2 illustrates the operation of the lenses. The object plane is located at the array center and the image plane is located at infinity (far-field). The lenses focus the fan beam from the phased array into a narrower spot beam. The beamwidth reduction ratio is equivalent to the focusing directivity [26]. In the far-field of the phased array feed PCBs, the wavefronts have a large curvature. As the wavefronts pass through these lenses, the curvature is reduced such that the outgoing wavefronts are more parallel. The remaining wavefront curvature determines the beamwidth of the resulting radiation pattern. The central lens is located in the radiative near-field of the phased array, where power is not predominantly stored. Both the central and inner side lenses are located at the same distance from the array center. However, the side lenses are located in the far-field of the array because the projected length of the array reduces in the direction of the maximum steering angle. As shown in Fig. 2(b), the wavefronts within this region are well-defined. They are also well-defined at boresight, as evidenced by Fig. 14(a) in Section V.

The lenses can be installed above an existing phased array incorporating amplitude control. The authors recently proposed a low-cost feed network suitable for millimeter wave phased arrays [27]. In this paper, we employ similar feed networks to drive the phased array. Four beam steering directions were chosen as a proof-of-concept. Practical beam steering systems would use a larger number of beam directions, determined by the resolution of the phase shifters connected to the radiating elements.

A different amplitude distribution is applied for each steering angle θ_0, as described in Section III.D. For most steering angles, including boresight ($\theta_0 = 0°$) and the maximum steering angle θ_{0max}, we apply a Taylor distribution to the amplitude excitations for the phased array to reduce the SLL [2]. When steering towards boresight, the elements are excited in phase ($\beta = 0°$ where β is the progressive phase shift between elements), and the central lens focuses the radiated fields. When steering to θ_{0max}, the side lenses focus the wavefronts.

When steering using phase-only control to angles that would place the beam between the central and side lenses ($\theta_0 = \pm20°$ and $\pm40°$), unwanted diffraction splits the main lobe. In order to prevent the main lobe from splitting, and correctly illuminate the lenses, the phased array must generate shaped beams. For the first time we employ novel asymmetric (special) amplitude distributions when steering to angles between the lenses. Using these distributions, we select elements that provide a main lobe which aligns with the desired steering direction. This ensures that, when steering between the lenses, the separate beams from the feeding antenna recombine into a single main lobe in the far-field.

The term *focused element factor* is used here to refer to the radiation pattern of an individually excited element, after it has been focused by the system of lenses. In this design, each focused element factor exhibits several main lobes, due to the presence of several lenses pointing towards different directions. These are used in order to achieve coverage of the sector. The beamwidth of each focused element factor becomes narrower as the scan angle increases. This property is used in this design to overcome beamwidth broadening. In this way the antenna is able to cover the entire steering range with an acceptable level of gain. The steering performance is illustrated in Fig. 3.

III. DESIGN PROCEDURE

In this section, we describe a design procedure for calculating the physical dimensions and material properties of the antenna, to achieve a particular operating frequency f_0 and antenna gain G_{req}. Firstly, a phased array is designed to achieve the required boresight gain, and the required focusing gain of the lenses is evaluated as a function of steering angle. Then, the lens positions, physical dimensions and materials are determined, and the focused element factors are calculated or simulated. Finally, for each beam steering angle, we calculate the amplitude and phase excitations to be applied to the phased array elements. These excitations are implemented using feed networks incorporating unequal power dividers. Equations (4), (8)-(12) and (18)-(20) are presented for the first time.
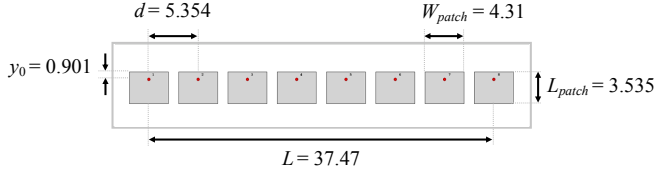
Fig. 4. Phased array with 8 elements. Dimensions are given in mm.

(a)   (b)

Fig. 5. 8-element Taylor $\beta = 144°$ array illuminating a large Fresnel zone plate lens with 6 zones, tilted to an angle of 53.1°. (a) Physical structure, (b) Simulated radiation pattern, showing realized gain in dBi.

A. Antenna Requirements and Phased Array Design

TABLE I
ANTENNA SPECIFICATION FOR USE IN A 5G BASE STATION

Criterion	Value
Gain	17 dBi
Beamwidth (azimuth)	17°
Beamwidth (elevation)	20°
Sidelobe Level	-10 dB (for SINR of 7 dB)
Steering range per sector (azimuth)	±60°
Steering range per sector (elevation)	0° to +70° (35° downtilt)
Number of sectors	3
Beams per sector	1. Multibeam in later design
Frequency band (UL and DL)	27.5 – 29.5 GHz
Data rate per sector (SISO)	2 Gbps, assuming OFDM
Tracking speed (moving user)	0 - 120 km/h
Pointing accuracy (azimuth)	±2.5°

Table I summarizes the antenna requirements for a typical 5G scenario. The center frequency f_0 = 28 GHz was selected, as it is a candidate band for 5G in the US, Korea, and Japan [28]. The third generation partnership programme (3GPP) and ETSI have both prepared standards for the 5G new radio (NR). However, there is currently no 3GPP or ETSI specification on for the beamwidth of a millimeter wave (i.e. type 2-O) base station other than for satellite terminals and fixed links. A link budget was calculated for the chosen application. For a transmitted power of 0 dBm, a total boresight gain of $G(0)$ = 17 dBi is needed to yield a received power of at least -90 dBm at a link range of 200 m. The beamwidth specifications given in Table I were calculated based on the directivity value required to meet the link range requirements whilst also minimizing the pointing loss when tracking mobile users [1]. A rectangular microstrip patch of boresight directivity G_{EF} = 8 dBi was selected as the radiating element.

A half-wavelength element spacing ($d = \frac{\lambda_0}{2}$) produced a good compromise between mutual coupling and steering range. As shown in Fig. 4, the original array length is $L = (N-1)d$. We consider azimuth steering of a linear array, which could later be extended to elevation steering using a planar array. The azimuth steering range $\pm\theta_{0max}$ is calculated from [2]:

$$\theta_{0max} = \sin^{-1}(1 - 0.4429\lambda_0/Nd) \tag{3}$$

Our original antenna design did not meet the gain specification of 17 dBi mentioned in Table I. Following careful investigation, we discovered that mutual coupling of up to -16.1 dB between the array elements reduced the peak gain in the boresight direction by $D_{coupling}$ = 1.63 dB.

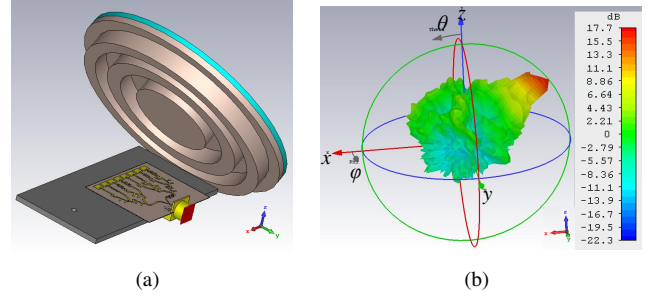Similarly, the taper efficiency of the Taylor distribution [2] as well as amplitude and phase errors within the feed networks [27] reduce the directivity by 0.56 dB and 0.3 dB, respectively. To account for these effects, the required number of elements in the phased array feed PCBs must be increased to: $N = \lceil 10^{(G(0)-G_{EF}+D_{coupling}+D_{Taylor}+D_{errors})/10} \rceil = 15$. This larger array could be implemented as two rows of 8 elements. As the rows point in different elevation directions beneath the lenses, co-phasing of +30° and -30° between rows is required to produce a 17 dBi beam.

Several losses within the antenna (e.g. conductor and dielectric loss) are independent of the steering angle. The value of the conductor and dielectric losses associated with the feed network L_{feed} = 0.66 dB was obtained accurately via simulation [27], rather than via calculations, as the accuracy of the latter would be impaired by the various assumptions required. Other losses such as the efficiency of the microstrip patches (0.8 dB), tapered transition (0.2 dB), and the lens matching layers (0.62 dB) must also be accounted for. In order to compensate for the total loss L_{total}, at least one inner lens, of focusing gain G_1 = 2.55 dB, is required at all steering angles.

In order to overcome scan loss, the antenna must ideally restore the gain, at any angle, to the value obtained at boresight, using equation (5). This gain increase $G_{req}(\theta_0)$ is proportional to the reciprocal of the scan loss, from (1). It has been quantized into discrete angular steps, each corresponding to the position of one or more lenses.

$$G_{req}(\theta_0) \propto G_1 \cos^{-1.5}(\theta_0) \tag{4}$$

where G_1 is the focusing gain of a single inner lens.

B. Lens Design: Physical Dimensions

To prevent blockage between adjacent lenses, we must minimize the angular and axial overlap between the central and side lenses. This is prevented by selecting an appropriate number of inner lenses N_{inner}, and maintaining an axial separation greater than the lens thickness.

The zone radii r_{ij} of the inner lenses are given by [29]:

$$r_{ij} = \sqrt{F_j\lambda_0 i + \left(\frac{\lambda_0 i}{2}\right)^2} \tag{5}$$

where integers i = 1 to N_{zones} and j = 1 to M.

Fig. 7 shows front and side views of an inner lens. Its focal length is $F_1 = 20$ mm. The F/D ratio helps to determine the trade-off between gain and steering range [30]. Each lens has the same number of zones N_{zones}. We selected $F/D = 0.4$ and $N_{zones} = 2$ to limit the lens diameter D_j, as mentioned earlier. As shown in Fig. 5, a single lens of larger diameter is able to produce the required focusing gain, but would obstruct the beam when steering to boresight. For this reason, cascading is employed. For the inner lenses, $m = 1$. Next, we calculated the inner lens diameter D_1 [29] and the subtended angle as $\theta_{sub} = \tan^{-1}(D_1/2F_1) = 51.3°$ [31].

$$D_j = 2\sqrt{F_j \lambda_0 N_{zones} + (\lambda_0 N_{zones}/2)^2} \qquad (6)$$

F_j is the focal length of a lens at cascading depth j. The angle between the center of each lens k and the array normal (z-axis) is given by:

$$\theta_k = \theta_{0max}(k - (N_{inner} + 1)/2) \qquad (7)$$

where $k = 1$ to N_{inner}. In this design, $N_{inner} = \lfloor 180°/\theta_{sub} \rfloor = 3$, so there is a lens at boresight and at $\pm\theta_{0max}$. Each lens covers an angular range $\theta_k \pm \frac{\theta_{sub}}{2}$.

Here, we design the lens combination with the aim of achieving the required gain. As shown in Fig. 7, F_1, F_2, F_3 are the focal lengths of the individual lenses, with diameters D_1, D_2, D_3.

The term *cascading depth*, $M(\theta_0)$, refers to the number of lenses arranged along a straight line pointing outwards from the array center at an angle θ_0. The insertion loss of the matching layer material, $\alpha_{match} = \frac{\pi}{\lambda_0}\tan\delta$ Np/mm $= 8.686\frac{\pi}{\lambda_0}\tan\delta$ dB/mm [32], causes exponential decay $e^{-2M\alpha_{match}t_{match}}$ of the signal power. As M is increased, this insertion loss increases[1]. However, the focusing directivity also increases, provided that the outer lenses are positioned appropriately such that the focal point of the cascaded zone plate triplet is located at the center of the phased array. More insertion loss could be tolerated if the directivity of each lens is increased.

Let us define a matching layer loss threshold $\alpha_{threshold} = 1/(4t_{match})\ln(\sqrt{3}G_1)$. If the loss constant α_{match} is above this threshold, adding more lenses (increasing M) will reduce the gain. Let us rearrange the straight-line equation describing the data points in the inset to Fig. 6. The resulting equation describes the threshold in terms of the loss tangent: $\tan\delta < (14.616 - G_{nolenses})/58.439 = 0.0829$. The realized gain resulting from this trade-off is visualized in Fig. 6, for 1, 2, or 3 side lenses. In Fig. 6, when $M = 2$, the blue lines correspond to the inner and middle lenses, and the other lines correspond to the inner and outer lenses. Removing the middle lens yields a gain increase of 3.32 dB. This was discovered after the antenna had been fabricated.

All of the side lenses are scaled copies of the inner lens, which has focusing gain G_1. If G_1 is increased, the loss threshold (to achieve a target gain value $G_{req}(\theta_0)$) increases, so fewer lenses are needed to achieve the target gain.

$$G_{req}(\theta_{0max}) = G_1 \cos^{-1.5}(\theta_{0max})e^{2M\alpha_{match}t_{match}} \qquad (8)$$

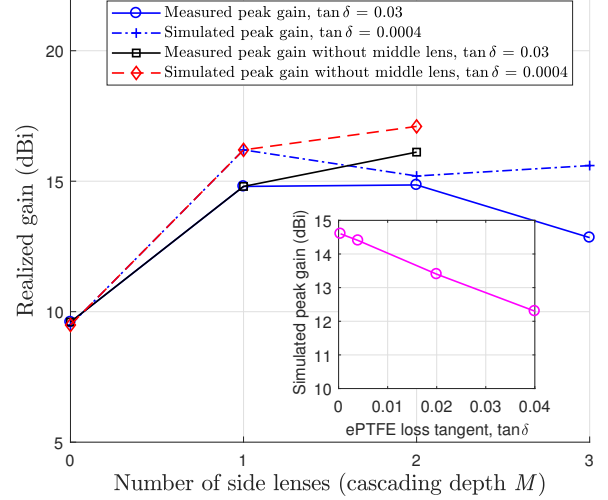[1]The total matching layer loss is $2ML_{match} = 2M\alpha_{match}t_{match}$.

Fig. 6. Simulated and measured peak gain vs. cascading depth M (number of side lenses) for the Taylor $\beta = 144°$ PCB, for different values of matching layer loss tangent. Inset: Effect of matching layer loss tangent $\tan\delta$ on simulated peak gain, for $M = 3$.

For the fabricated design, we selected a cascading depth value $M = 3$.

$$G_{req}(\theta_{0max}) = G_1 \frac{F_3}{F_2} \qquad (9)$$

Now we calculate the focal lengths. Recall that the cascaded lens arrangement aims to achieve a greater gain increase (focusing gain) than could be achieved using a single lens, whilst maintaining the same back focal length F and subtended angle[2]. When $M = 3$, for refractive lenses, F can be expressed as [24]:

$$F = \frac{\frac{F_1 F_2}{F_1 + F_2 - d_{12}}F_3}{\frac{F_1 F_2}{F_1 + F_2 - d_{12}} + F_3 - d_{23}} \qquad (10)$$

where the separations between side lenses are $d_{12} = F_2 - F_1$ and $d_{23} = F_3 - F_2$. We assume that the distance from each lens to the array center is equal to its focal length. The focal length of each lens is chosen so that $F = F_1$. Substituting this into (10) and rearranging gives $F_3 = 3F_1$. Combining this with (9) gives the value of F_2:

$$F_2 = 3F_1 \frac{G_1}{G_{req}(\theta_{0max})} \qquad (11)$$

If the lenses are thin, F_2 can be adjusted to set the focusing gain. For values of M larger than 3, the focal length of an arbitrary number of cascaded lenses can be calculated using (10) recursively. The radial dimensions of the lenses (Table II) increase with distance from the array center. The ratio of the

[2](9) - (11) are not claimed to be exact equations designed from electromagnetic field theory. They are approximate models based on the thin-lens assumption [36]. It was later found that the focal point is closer to the rear surface of the inner lens than expected. This is due to the focal shift effect which occurs for Gaussian beams [25]. In Section V, the outer lens was repositioned to compensate for this effect. A more accurate model based on diffraction is available in [16].

TABLE II
LENS ZONE RADII r_{ij} (MM)

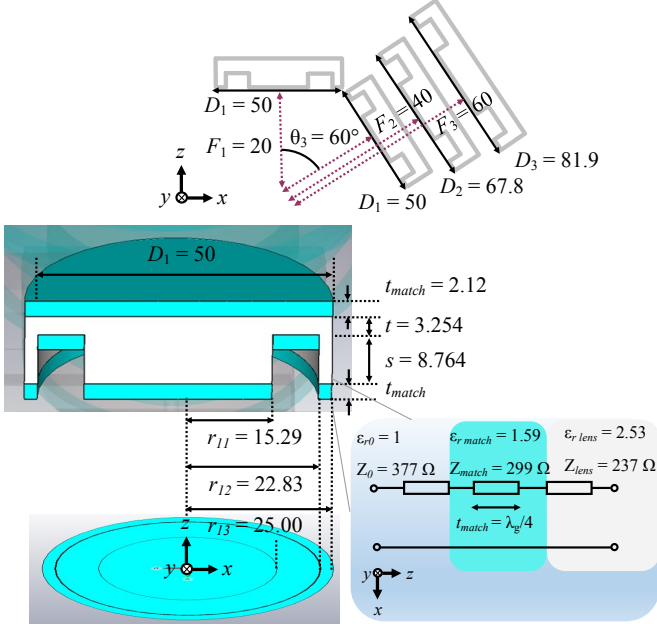|		Lens 1	Index 2	i 3
Zone	1	15.29	20.74	25.05
Index	2	22.83	30.96	37.40
j	3	25.00	33.90	40.95

Fig. 7. Lens dimensions in mm, including a cross-section through the central lens. Inset: equivalent circuit an interface between air, one matching layer, and Rexolite. Impedance values are valid for the middle and outer side lenses.

outer lens zone radii to the inner lens zone radii is equal to the ratio of the lens diameters D_j:

$$r_{ij} \approx \frac{D_j}{D_1} r_{i1} \tag{12}$$

The lens zone radii could be more accurately calculated using (6).

C. Lens Materials, Thickness and Groove Depth

To simplify the design, we assumed a lossless dielectric ($\tan \delta = 0$, i.e. $\epsilon''_{rlens} = 0$). The lens depth dimensions are given by [29]:

$$s = \frac{\lambda_0}{2(\sqrt{\epsilon_{rlens}} - 1)} \tag{13}$$

$$t = \frac{\lambda_0}{2\sqrt{\epsilon_{rlens}}} \tag{14}$$

The matching layers act as quarter wave transformers to minimize reflections (Fig. 7 inset). As the wave propagates through the layers, the wave impedance $Z = \frac{|\boldsymbol{E}|}{|\boldsymbol{H}|}$ decreases through the air-ePTFE-Rexolite interfaces, then increases from
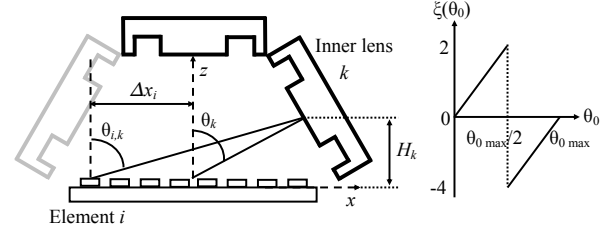

Fig. 8. Antenna geometry: variation in element positions causes a variation in the focused EF main lobe directions.
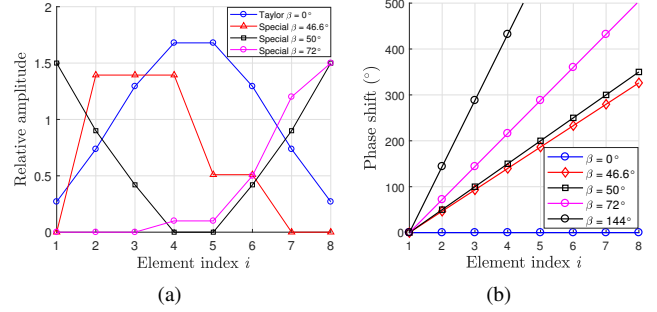

Fig. 9. Amplitudes and phases for Special and Taylor excitations. The amplitudes are then normalized to the same total power for each beam direction. (a) Amplitudes, (b) Phases.

the lens to free-space[3]. The ideal permittivity $\epsilon_{rmatch} = 1.59$ and thickness $t_{match} = 2.12$ mm are calculated using (15) and (16) [32].

$$\epsilon_{rmatch} = \frac{Z_0}{Z_{lens}} = \sqrt{\epsilon_{rlens}} \tag{15}$$

$$t_{match} = \frac{\lambda_g}{4} = \frac{\lambda_0}{4\sqrt{\epsilon_{rmatch}}} \tag{16}$$

The values of parameters s, t, ϵ_{rmatch} and t_{match} depend only on λ_0 and ϵ_{rlens}, so are the same for all of the lenses. $Z_0 = 377$ Ω is the impedance of free-space.

D. Amplitude and Phase Distributions

Previously, microstrip feed networks were designed to implement a Taylor amplitude distribution and set the phases at the elements [27]. Here, we design feed networks to realise special amplitude distributions. More power is assigned to elements whose focused EFs align with θ_0. As θ_0 increases, from 0° to θ_{0max}, most of the input power is initially assigned to the elements for which $x < 0$, then to elements at $x > 0$.

The asymmetric element amplitudes $a'_i(\theta_0)$ are calculated using a skewed Taylor distribution. To skew a conventional

[3]Consider a radial line extending outwards from the centre of the phased array feed PCB. The wave impedance, along this line, varies as a function of the distance. It also varies with the angle of incidence from each array element to each lens. However, these effects are small, because the Taylor amplitude distribution ensures that most of the power is assigned to a subset of elements in the center of the array. Due to the proximity of the inner lenses to the phased array, near-field effects significantly increase the wave impedance at all points in space within the near-field region. However, as this effect scales the impedance of all materials equally, the reflections within the matching layers still cancel, and so inner lenses are still matched to the phased array.
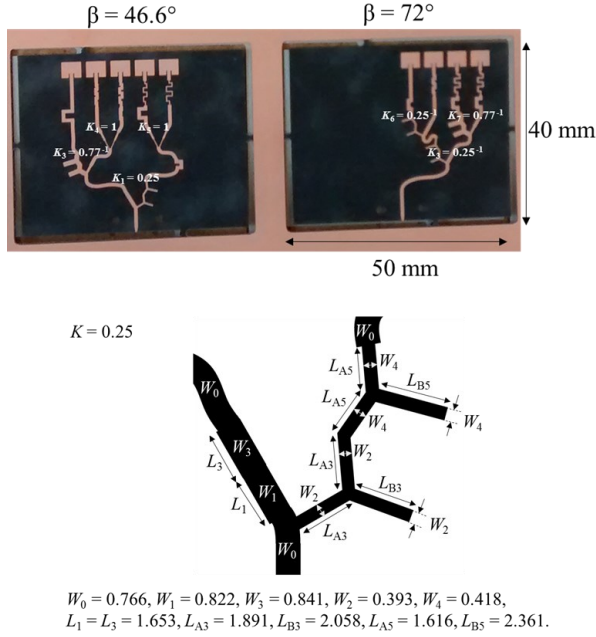
Fig. 10. Special PCBs: Voltage split ratios K_i and physical dimensions in mm (above), $K = 0.25$ unequal power divider (below).

Fig. 11. Photo of the fabricated antenna. Inset: side view showing a feed printed circuit board (PCB) beneath the lenses.

Taylor distribution a_i [27], we multiply it by an exponential decay or growth (which is sampled at N equally spaced points, where $i = 1$ to N):

$$a_i'(\theta_0) = a_i e^{-3\xi(\theta_0)d\left(i - \frac{N+1}{2}\right)} \tag{17}$$

The skewing parameter ξ represents the asymmetry (to the left if $\xi > 0$, to the right for $\xi < 0$). Let us consider the case when $N_{inner} = 3$. As shown in Fig. 8, ξ changes sign at $\theta_0 = \frac{\theta_{0max}}{2}$, so has a sawtooth shape.

$$\xi(\theta_0) = -2.5\tan^{-1}\left(\cot\left(\frac{\pi\theta_0}{\theta_{0max}} - \frac{\pi}{2}\right)\right) \tag{18}$$

$$= \begin{cases} 2\frac{\theta_0}{\theta_{0max}} & \theta_0 < \frac{\theta_{0max}}{2} \\ 4\left(\frac{\theta_0}{\theta_{0max}} - 1\right) & \theta_0 \geq \frac{\theta_{0max}}{2} \end{cases} \tag{19}$$

To implement the amplitudes in Fig. 9, an unequal divider with a voltage split ratio $K = 0.25$ was designed (Fig. 10).

In the region between the central and side lenses, the progressive phase $\beta(\theta_0)$ was reduced by a factor of 0.65, so values $\beta = 46.6°$ and $72°$ were chosen for steering angles $\theta_0 = 14°$ and $40°$. These are shown in Fig. 9(b). β was implemented via meanders.

The phase at the element i is given by:

$$\phi_i'(\theta_0) = \begin{cases} -(\psi + 0.65kd\cos\theta_0)(i-1) & 20° < \theta_0 < 40° \\ -kd(i-1)\cos\theta_0 & \text{otherwise} \end{cases} \tag{20}$$

In order to achieve fine beam steering at the discontinuity between lenses (around $\theta_0 = 30°$), the Special $\beta = 50°$ amplitudes are used. For the phases, $\psi = 10(\theta_0 - 26°)$ if $i = 7,8$ or $\psi = 0°$ otherwise. Each value of ψ corresponds to a different fine steering of the beam direction θ_0.
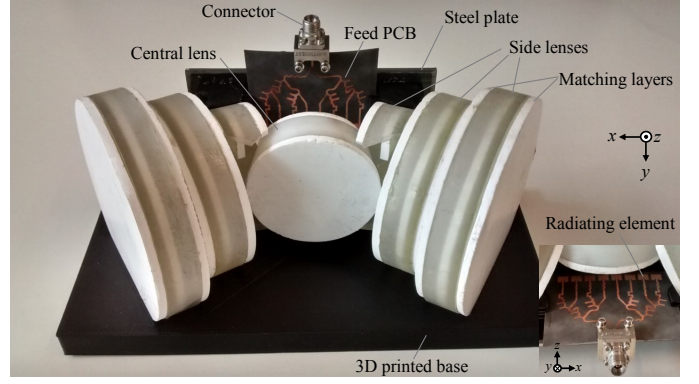
IV. PROTOTYPE FABRICATION

Fig. 11 illustrates the antenna prototype, fabricated using conventional low-cost manufacturing techniques. It is essential to select low-loss materials to maximize the total efficiency. Rexolite® 1422 was selected as the lens material ($\epsilon_{rlens} = 2.53$, $\tan\delta = 0.0001$ at 10 GHz). Its refractive index is $n = \sqrt{\epsilon_{rlens}} = 1.59$. For each lens, impedance matching layers of thickness $\lambda_g/4$ reduce reflections and improve the efficiency. They are made from expanded Teflon® (ePTFE, $\epsilon_{rmatch} = 1.4$ and $\tan\delta = 0.03$ at 10 GHz). ePTFE is available with a 3 mm thickness. It does not absorb water, so is suitable for outdoor applications. For each beam direction, a different PCB was designed. The PCBs were fabricated on Rogers® RT5880 substrate ($\epsilon_r = 2.2$, $\tan\delta = 0.0009$ at 10 GHz). To improve the front-to-back ratio, a metal plate reflector of thickness $\frac{\lambda_0}{4}$ was placed at a distance $\frac{3\lambda_0}{4}$ behind the array.

The side lenses were machined on a lathe. The central lens was CNC machined from HDPE ($\epsilon_r = 2.3$, $\tan\delta = 0.001$), a recyclable, low-cost plastic. The laser-cut matching layers were glued to the lenses using Araldite® epoxy resin. The lenses and steel plate were screwed onto the base, which was 3D printed from PLA ($\epsilon_r = 3.5$). 2.92 mm end-launch solderless connectors were screwed to the etched PCBs, which were slotted into grooves in the base, beneath the lenses. Movement along the x-, y-, and z-axes, and flexure of the phased array feed PCBs, can cause random errors in their physical alignment beneath the lenses. This affects the measured radiation pattern, so must be minimized. To improve measurement repeatability, we designed a fixture to hold the PCBs firmly in place and prevent bending, as far as possible.

The antenna dimensions are $180 \times 90 \times 82$ mm. Although electrically large, the proposed antenna yields an acceptable gain level over a moderately wide steering range, compared to a conventional phased array. This justifies its bulkier form factor, as it is intended for access points, rather than mobile handsets.

V. RESULTS

Fig. 12 presents the H field distribution and current density associated with the antenna, along with the resulting radiation patterns. These results were obtained through simulation in
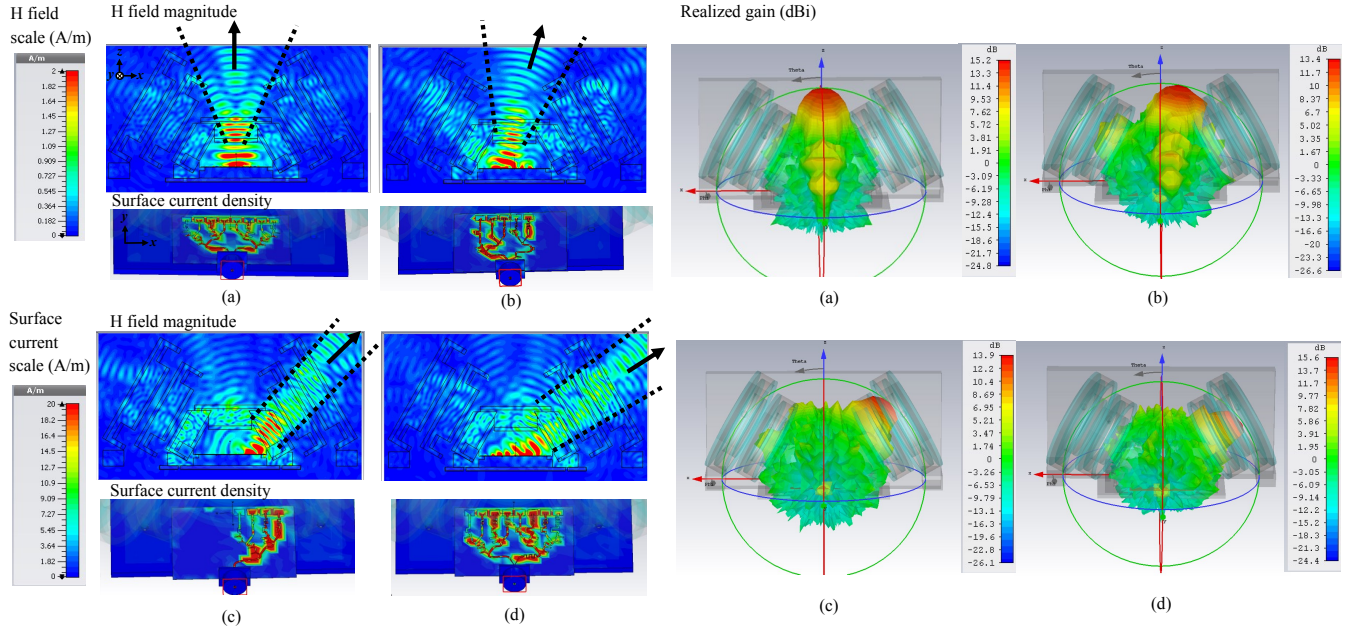
Fig. 12. Simulated H field cross-section, surface current density in the feed PCBs, and far-field radiation patterns. Results correspond to $\tan\delta = 0.0004$. (a) Taylor $\beta = 0°$. (b) Special $\beta = 46.6°$. (c) Special $\beta = 72°$. (d) Taylor $\beta = 144°$.
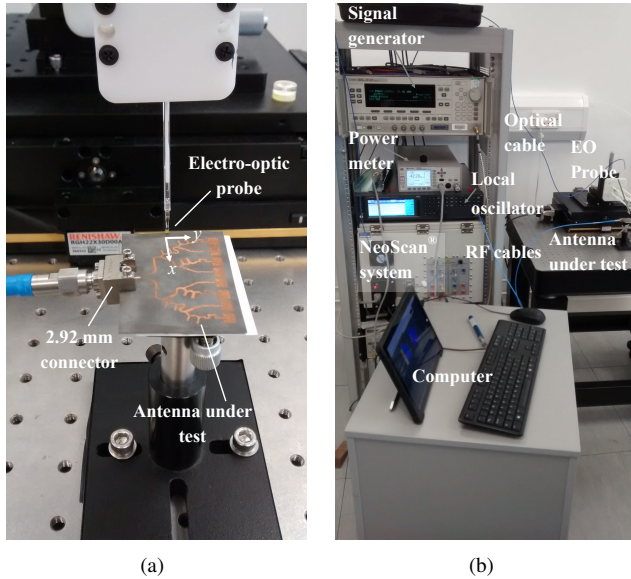

Fig. 13. Electro-optic probe measurement setup. (a) Probe above the antenna under test. (b) Lab equipment, including 2.92 mm RF and optical cables.
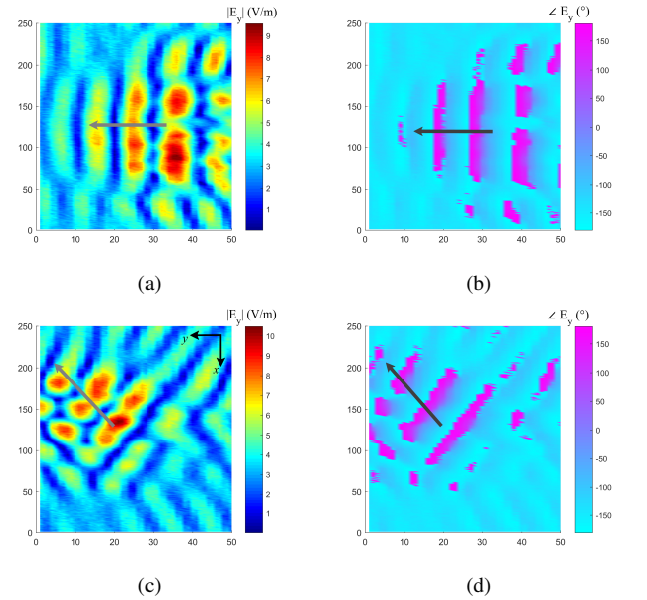

Fig. 14. Measured E_y-field magnitude (V/m) and phase (°), plotted against x and y directions in numbers of steps. A well-defined wavefront can be observed. (a) Taylor $\beta = 0°$ magnitude. (b) Taylor $\beta = 0°$ phase. (c) Taylor $\beta = 144°$ magnitude. (d) Taylor $\beta = 144°$ phase.

CST Microwave Studio® using the time-domain solver with a hexahedral TLM mesh. The input power is split within the feed network. The fan beam from the array is focused, by the lenses, into a spot beam.

In order to characterize the nature of the wavefronts produced by the phased array feed PCBs, we used an electro-optic (EO) probe [33] to measure the corresponding E_y fields. The probe was scanned at a distance of 1.5 mm above the surface of the PCBs, in 0.2 mm steps. Fig. 13 shows the test setup. The NeoScan® system contains mixers, amplifiers, and an optical detector. The local oscillator output power was set to 15 dBm

at 14.05 GHz. From the measured wavefronts presented in Fig. 14, we calculated the phase constants β_x and β_y. Using [9], we verified that the azimuth and elevation beam directions, ϕ_0 and θ_0, were as expected from simulation (Table III). This enabled us to establish that radiation from the feed networks does not significantly alter the main lobe direction of radiation, and hence that the lenses are being correctly illuminated.

Fig. 15 shows the measured return loss of the antenna. Although the resonant frequency varies between feed networks
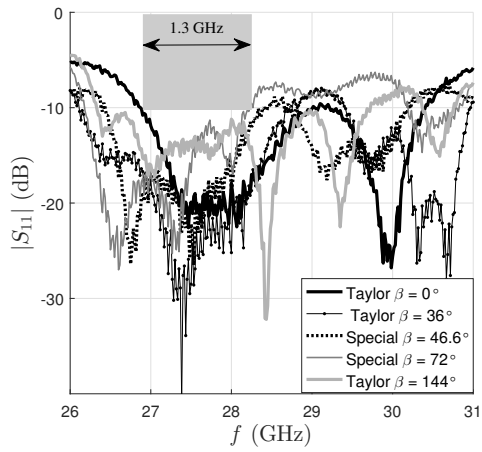
Fig. 15. Measured scattering parameters of the complete antenna assembly: PCBs with lenses and matching layers.
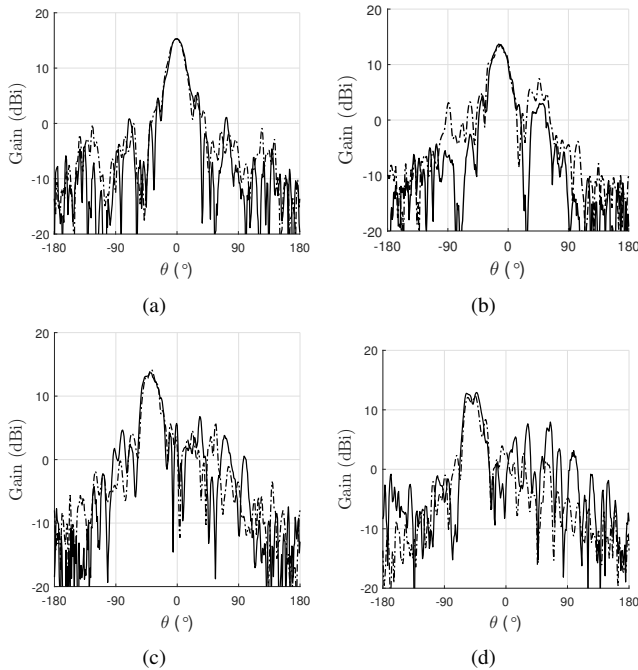

(a)

(b)

(c)

(d)

Fig. 16. Azimuth radiation patterns for the PCBs with lenses and matching layers. Simulated (dash-dot line) and measured (solid line). (a) Taylor $\beta = 0°$. (b) Special $\beta = 46.6°$. (c) Special $\beta = 72°$. (d) Taylor $\beta = 144°$.

due to the meanders, a -10 dB reflection coefficient bandwidth of 1.3 GHz is achieved for all steering angles. As the lenses are impedance matched to the phased array, they do not significantly change the load impedance experienced by the array. This was verified by measuring the reflection coefficient $|S_{11}|$ of the phased array PCBs both with and without the lenses.

Fig. 16 shows good agreement between simulated and measured radiation patterns. In Fig. 16(a), the boresight gain of 15.35 agreed well with the simulated value of 15.28 dBi. In Fig. 16(b) and 16(c), the special PCBs illuminated the lenses to produce gains of 13.68 dBi and 13.67 dBi respectively. This verifies the success of the calculated amplitudes. In Fig. 16(d), a measured gain of 12.96 dBi was produced by the lens antenna fed by the Taylor $\beta = 144°$ PCB. The loss tangent
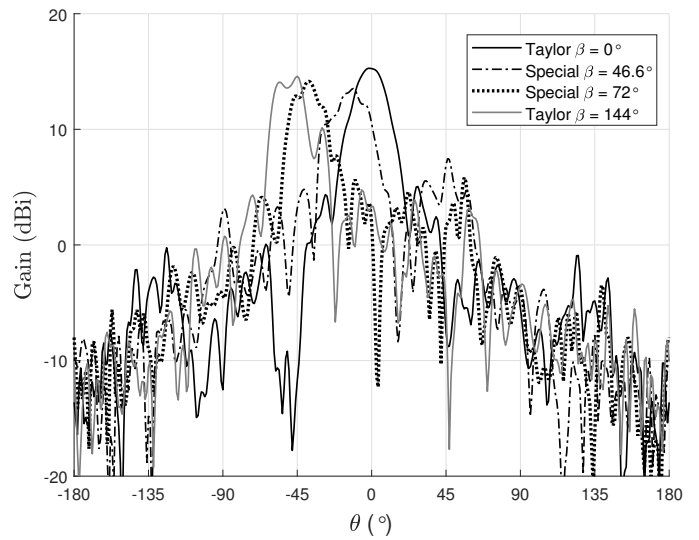
Fig. 17. Simulated azimuth radiation patterns for the PCBs with lenses and matching layers: all steering angles. Results correspond to $\tan \delta = 0.0004$.
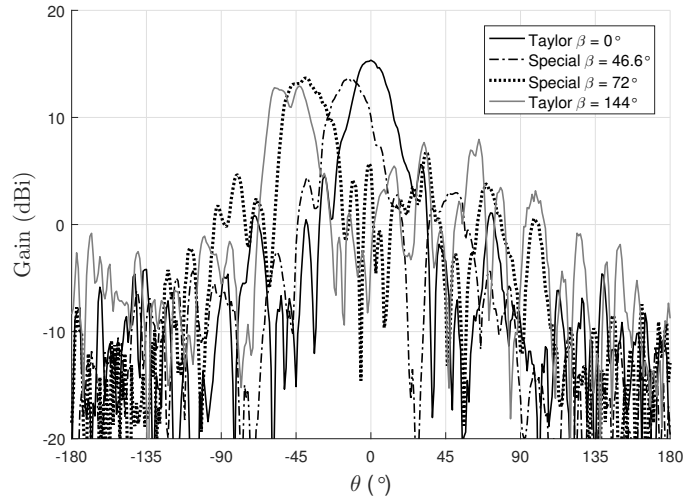
Fig. 18. Measured azimuth radiation patterns for the PCBs with lenses and matching layers: all steering angles. Results correspond to $\tan \delta = 0.03$.
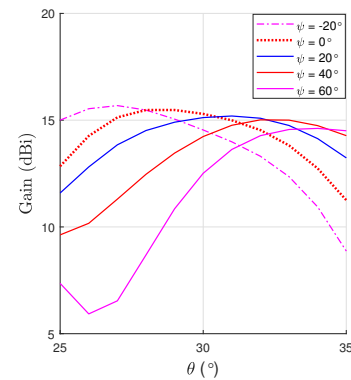
Fig. 19. Simulated azimuth radiation patterns for fine steering in the region between the central and side lenses, using the Special $\beta = 50°$ amplitudes.

value of 0.03 for the matching layer material (ePTFE), used in the prototype, was deduced by adjusting $\tan \delta$ in simulation until the simulated and measured main lobe gain agreed. This

Phased Array PCB	β_x (°)	β_y (°)	ϕ_0 (°)	θ_0 (°)
Taylor $\beta = 0°$	12.99	23.77	28.65	8.66
Taylor $\beta = 144°$	124.4	25.50	11.58	44.87

|	Achieved Steering Angle (°)	Gain (dBi)	Simulated Directivity (dBi)	Total Efficiency (%)	SLL (dB)
Taylor $\beta = 0°$	0	15.35	16.0	75.25	-9.74
Special $\beta = 46.6°$	14	13.69	15.1	79.27	-9.31
Special $\beta = 72°$	39	13.68	15.4	82.5	-6.90
Taylor $\beta = 144°$	52	12.96	16.0	62.5	-4.78

Fig. 20. Measured and theoretical realized gain vs. frequency for the Special $\beta = 72°$ PCB, showing acceptable bandwidth performance.

corresponds to the straight line fit in the inset to Fig. 6.

Fig. 18 shows the variation of the antenna gain across the steering range. The antenna has reduced the scan loss to 2.39 dB, and demonstrated a significant reduction in beamwidth broadening. If a low-loss matching layer material (i.e. $\tan \delta = 0.0004$) is employed, then simulations indicate that the scan loss can be reduced to 0.69 dB, as shown in Fig. 17.

Table IV summarizes the antenna performance. The boresight efficiency of 75.3% was calculated as the ratio between directivity (16.0 dBi) and measured boresight gain (15.35 dBi), adjusted by the ratio of the measured and simulated beamwidths. Despite the extra losses, an efficiency of 62.5% was achieved at $\theta_{0max} = 52°$. Additionally, the measured azimuth beamwidths of 21° / 24° / 27° / 26° agreed well with the simulated values of 24° / 22° / 22° / 20.5°, for the achieved steering angles of 0°, 14°, 39°, and 52° respectively (i.e. for $\beta = 0°$, 46.6°, 72°, 144°, respectively). When steering to the maximum angle, the measured elevation beamwidth was 15.7°, which meets the specification in Table I and demonstrates the focusing effect of the cascaded lenses. Beam steering with a measured crossover level of 10.0 dBi has been demonstrated in Fig. 18.

Fig. 19 presents the fine beam steering performance of the antenna in the region close to $\theta_0 = \pm 30°$. As described in Section III.D, this is implemented by adjusting the phases on elements 7 and 8. A simulated crossover gain of 14.75 dBi is achieved when a larger number of beam directions is considered. Further discussions on crossover gain can be found in [34].

The boresight gain of the conventional phased array in isolation (without the lenses) was 11.9 dBi [27]. The scan loss of the conventional phased array is 3.13 dB and the maximum scan angle was $\theta_{0max} = 49°$ (for $\beta = 144°$). For the novel antenna, reported here, the lenses increase the gain by 2.45 dB at boresight, and by 3.19 dB at $\theta_{0max} = 52°$. With the lenses, the average gain is 3 dB higher than for the phased array in isolation.

From the results in Table IV we see that the proposed antenna exhibits 2.39 dB of scan loss (i.e. 0.74 dB lower than that of the phased ar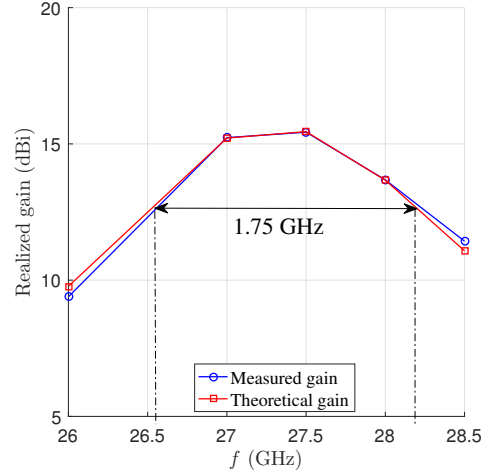ray in isolation), along with a significant reduction in beamwidth broadening. The reduction in scan loss was less than anticipated, because the loss tangent of the low-cost ePTFE matching layer material was 0.03, which is much higher than expected. If a low-loss matching layer material (i.e. $\tan \delta = 0.0004$) is employed, then simulations indicate that the scan loss can be reduced to 0.69 dB (i.e. 2.44 dB lower than that of the phased array in isolation).

The measurements have emphasized several important design aspects. Using the steel plate reflector, a front-to-back ratio of at least 19.75 dB was achieved for steering angles up to $\pm 39°$. When measuring the uniform PCB with lenses (not shown), the boresight SLL was -6.2 dB, whereas using the Taylor PCB, it was -9.74 dB. Hence, the Taylor distribution has reduced the SLL.

Fig. 20 displays the measured antenna gain $G(f)$ (dBi) versus frequency, f in GHz. Eq. (21) was empirically derived by curve fitting to a result obtained via measurement. The measured 3 dB gain bandwidth of 1.75 GHz is sufficiently wide for 5G applications, such as small-cell millimeter wave access points, and satellite communication from ships, aircraft, and trains. The bandwidth could be increased further through the use of stacked patch elements, to cover the 26 GHz European band [35].

$$G(f) = 20 \log_{10} \left(\left(\frac{\sin (0.28f)}{0.28f} \right)^2 \frac{1}{\sqrt{1 + (f - 27.25)^2}} \right) + 51.4 \tag{21}$$

The frequency performance of Fresnel zone plate lenses has been extensively analyzed in the literature [37]. As the number of zones is reduced, the depth of focus increases, and the bandwidth increases. This justifies the small number of zones $N_{zones} = 2$ used in this design, and verifies that the lenses and matching layers are wideband.

The main lobe of the steered radiation pattern, associated with the original design, is distorted. This defocusing is due to the focal shift effect which occurs for Gaussian beams, as described earlier in Section III.B. Following detailed investigation, we discovered that this distortion can be reduced by optimising the positions of the lenses in the triplet. In
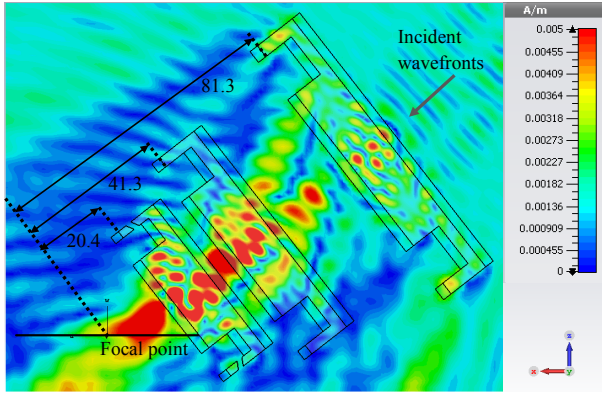
Fig. 21. Repositioning of the side lenses to focus on the center of the phased array, when steering to the maximum angle. Physical dimensions are in mm. H-field magnitude, showing that the focal point is at the origin.
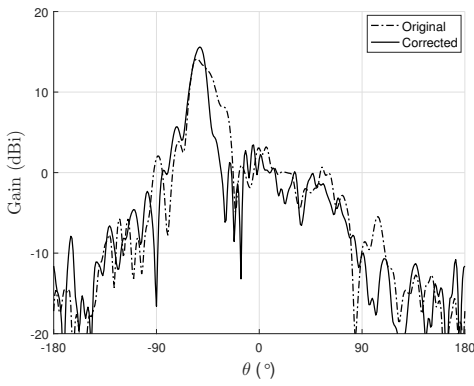

Fig. 22. Simulated azimuth radiation patterns, for the original and improved designs, fed by the Taylor $\beta = 144°$ PCB.

the original fabricated design, the side lenses were positioned 20 mm, 40 mm, and 60 mm away from the center of the phased array, respectively. In an improved design, these values have been adjusted to 20.4 mm, 41.3 mm, and 81.3 mm, respectively. The lens tilt angle is reduced from 60° to 52°, and the diameter of the outer lens is increased by 5%. As shown in Fig. 21, the focal point is now located towards the centre of the phased array. With this enhancement, the scan loss is reduced to 0.89 dB, and the simulated gain, at the maximum steering angle, has increased to 15.6 dBi. This is shown in Fig. 22, which corresponds to illumination by the phased array. For further details of the focusing effect of the lenses, see Supplementary Figs. 1 and 2. Table V summarises the scan loss reduction performance for each of the presented designs.

VI. DISCUSSION

Table VI provides a comparison with state-of-the-art designs, according to the performance criteria in Table I. These designs employ electronic beam steering, and have a single input port. To enable fair comparison between designs having different array sizes and operating frequencies, we derived a formula to normalize the gain performance: $G' = G - 10\log_{10}(\frac{1}{2}N_2 M_2 p_{x2} p_{y2})$, where N_2 and M_2 are the number of array elements, and p_{x2} and p_{y2} are the ratios of

Design	Scan loss (dB)	Difference (dB) compared to phased array
Isolated phased array	3.13	0
Proposed antenna with ePTFE ($\tan\delta = 0.03$) matching layers	2.39	0.74
Design with repositioned lenses and ePTFE ($\tan\delta = 0.03$) matching layers	0.89	2.24
Proposed antenna with low-loss ($\tan\delta = 0.0004$) matching layers	0.69	2.44

element spacing to wavelength, in the x- and y-axis directions, respectively.

Impressive steering performance was recently achieved using a spherical lens [18]. However, due to the positions of the radiating elements, long transmission lines were required. These incurred a large insertion loss, thus reducing the total efficiency of the antenna and increasing the scan loss. Parasitic elements, and widely-spaced elements within interleaved arrays, can be used to increase the gain and reduce the SLL of a 1D array [35]. This technique could be combined with our proposed lenses. As our design only feeds the elements from a single direction, it can more easily produce a spot beam, as required by the 5G specification in Table I.

When compared with state-of-the-art designs, the trade-off between gain and steering range depends on several factors, including the number of elements and the directivity of those elements. Designs using more directional elements tend to have a higher boresight gain, but a reduced steering range, for example [6] and [38]. In order to increase the boresight gain of the proposed design, to meet the target value of 17 dBi, the number of array elements must be doubled. The finite size of the lens focal region limits the number of elements and thus the maximum achievable gain, however it is sufficiently large to accommodate these additional elements.

The proposed design offers three main advantages: high average gain, low scan loss, and a moderately wide steering range[4] of ±52°. These make it suitable for use within 5G small-cell access points. Additionally, by using phased arrays, the design avoids the need for a complex and costly switch matrix such as that used in [18].

The estimated mass-manufacturing cost of the antenna, including amplitude and phase control ICs, is almost 50% lower than that of a spherical lens antenna [18], but around 26% and 22% higher that of an equivalent isolated phased array [27] or a metamaterial based antenna [6], respectively. This additional cost is justified, given the advantages discussed above.

The main disadvantage of the proposed antenna design is its high SLL. The high SLL at boresight is primarily caused by lobes in the array factor of the feed PCBs, which are increased by amplitude and phase errors. At the maximum steering angle, θ_{0max}, radiation from the feed increases the SLL. To

[4]In the fabricated prototype, the useful steering range for which the SLL is below -9 dB is ±14°. This is because the lenses magnify both the main lobe and the sidelobes. However, if the steering range is defined in terms of gain, it can be expressed as ±52°.

TABLE VI

COMPARISON WITH THE STATE-OF-THE-ART

Design	Operating Frequency (GHz)	Number of elements	Scan angle range (°)	Measured boresight gain (dBi)	1D Scan loss at 50° (dB)	Maximum SLL (dB)	Equivalent boresight gain (dBi)
This work	28	8	±52	15.35	2.39	-4.78	15.35
[7]	28	7	±30	19	6	-12.1	19.56
[38]	5.2	64	±75, ±75	19	1.5	-10	11.38
[11]	77	33	±90, 0-20	28	0	-15	16.17
[18]	71	16	±40	19.6	3.8	-14	11.26
[35]	28	16	±49.5	19.88	1.18	-12.1	16.38

reduce the amplitude and phase errors in the feed PCBs, the power dividers and meanders within the feed networks could be iteratively optimised across a wide bandwidth. In a real implementation, we would employ amplifiers and phase shifters at each element with a high resolution, to reduce quantisation errors. In order to reduce the feed radiation, a non-radiative feed technology, such as substrate integrated waveguide (SIW) or stripline could be used. This would increase the manufacturing cost and complexity.

The approach can be extended to accommodate a planar array. 2D beam switching could be achieved by placing several linear arrays in parallel in the y-direction beneath the proposed lens configuration. The radiating elements in those arrays would be probe-fed from behind the ground plane. By digitally switching between the arrays, this configuration can be used to achieve elevation beam switching from -20° to +20°.

The proposed antenna has several possible applications, both within and beyond the field of mobile communications. Potential 5G applications include: 1) wireless access points, and 2) satellite user terminals, such as those mounted on the roof of a building, vehicle, or aircraft. These require beam steering, whilst maintaining high gain up to wide steering angles. Reconfigurable lenses could be used to reduce the form factor [40].

By increasing the signal-to-interference-and-noise ratio (SINR) of the received signal compared to a conventional phased array, this antenna could improve the link budget performance of a 5G system [41], especially for users located at azimuth angles in between sectors. At low SINR values, the capacity increases linearly with SINR [42]. Hence, this antenna could increase capacity (i.e. data rates) for users at the cell edge. A low SINR is also often observed at wide steering angles in low Earth orbit (LEO) satellite terminals, due to the high noise temperature of the 'hot' Earth [43]. By increasing the gain (received signal power) in these directions, the proposed antenna could greatly help to overcome this noise issue.

The lenses could be reshaped to better approximate an ideal phase distribution [39] [26]. If curved lenses were used instead, as in [15] [14], the focusing performance could be greatly improved, to meet the required specification. This would require more sophisticated simulations and costly precision machining. An improvement to the design was described in Section V. After repositioning the lenses, to optimise the design, the gain increased by 1.5 dB.

VII. CONCLUSION

A beam steerable millimeter wave antenna operating at 28 GHz has been presented. The antenna is designed to increase the gain at wide steering angles. For the first time, it incorporates a cascaded system of 7 Fresnel lenses fed by a 1×8 element phased array. By tilting the side lenses, the projected area is increased, and by cascading them, a higher focusing gain can be achieved whilst avoiding blockage of the central lens. A hardware prototype of the antenna was fabricated and measured. The directions of the wavefronts from the feed PCBs, illuminating the lenses, were verified using an electro-optic probe. In the fabricated design, the inner lenses produced the majority of the focusing gain, and the middle and outer lenses had less effect. The inner lenses increased the gain of the antenna by 2.45 dB at boresight, and by 3.19 dB at the maximum steering angle of ±52°. The antenna prototype achieved a 3 dB gain bandwidth of 1.75 GHz. At the maximum steering angle, the measured beamwidths were 26° and 15.7° in azimuth and elevation respectively. The scan loss was reduced to 2.39 dB. If a low-loss matching layer material (i.e. $\tan \delta = 0.0004$) is employed, then simulations indicate that the scan loss can be reduced to 0.69 dB. After repositioning the lenses, to optimise the design with lossy matching layers, a simulated gain of 15.6 dBi was achieved at the maximum steering angle, and the simulated scan loss was reduced to 0.89 dB. When steering to angles that place the beam between lenses, special amplitude distributions were applied via the phased array feed networks, to prevent the main lobe from splitting. This involves selecting elements whose focused patterns aligned with the beam steering direction. By mitigating scan loss, users will benefit from an increase in received signal power. A design procedure along with a theoretical analysis of diffraction through the lenses has been presented. In future work, the cascaded lens antenna concept could be extended to a MIMO scenario.

APPENDIX: DERIVATION OF THE FOCUSED ELEMENT FACTORS

We now derive the focused EFs from diffraction theory. For the first time, we combine focusing effects from multiple lenses in (27) and (28). The middle and outer side lenses are in the far-field of the radiating elements, so we can approximate their focusing behavior as Fraunhofer diffraction. As the inner lenses are located within the near-field of the phased array antenna, the wavefronts will be paraboloidal. Fresnel integrals [36] [23] could be used to more accurately

model this effect, accounting for interference between wavelets of varying phases.

A. Single Lens

Let us define a local Cartesian coordinate system x'-y', with its origin at the lens center. Each groove in the lens produces a $180°$ phase reversal $\Delta\phi = \frac{2\pi}{\lambda_0}(\sqrt{\epsilon_r}-1)s$ relative to the lens center [8]. This produces the minus sign in the formula below. The focused wavefronts are approximately parallel to the x'-y' plane, with uniform phase.

By superposition, the phase $\phi(r)$ of a single lens is a sum of circular apertures [45]. For a lens with two zones:

$$\phi(r) = \text{circ}\left(\frac{r}{r_1}\right) - \text{circ}\left(\frac{r}{r_2}\right) + \text{circ}\left(\frac{r}{r_3}\right) \quad (22)$$

where $r = \sqrt{x'^2 + y'^2}$ and $\text{circ}(r)$ is the circular function, with a value of 1 if $r < 1$, and 0 otherwise.

Diffraction through a circular aperture can be approximated by integrating the E-field over x' and y'.

$$G(u,v) = \int_{-\infty}^{+\infty}\int_{-\infty}^{+\infty} \phi(r)e^{-\text{j}2\pi(ux'+vy')}\,\text{d}x'\,\text{d}y' \quad (23)$$

where u and v are the angular spatial frequencies corresponding to x' and y' respectively.

To simplify the calculation, we change from Cartesian to polar coordinates [36].

$$G(r) = \int_0^{r_0}\int_0^{2\pi} \phi(r)e^{\text{j}kr\cos(\rho-r_0)}\rho\,\text{d}\rho\,\text{d}r \quad (24)$$

Substituting (22) into (23) and transforming to a 3D polar system, we obtain the azimuth pattern of a single microstrip patch antenna beneath a single lens. It is a sum of Airy disks, expressed in terms of Bessel functions, $J_1()$ [36] [26].

$$G_{kj}(\theta) = \cos^{1.5}\theta\left(\frac{1}{3}\left(\frac{J_1(l_1)}{l_1} - \frac{J_1(l_2)}{l_2} + \frac{J_1(l_3)}{l_3}\right)\right) \quad (25)$$

where $l_i = \frac{r_{i1}\sin(\theta)}{1.22\lambda_0}$. r_{ij} was defined in (6).

B. Multiple Lenses

As shown in Fig. 8, each element i is displaced $\Delta x_i = \left(i - \frac{N+1}{2}\right)d$ from the center of the array. The angle $\theta_{i,k}$ between element i and the center of lens k is calculated from the side lens height $H_k = F_1\cos\theta_k$.

$$\theta_{i,k} = 90 - \tan^{-1}\left(\frac{1}{\tan\theta_k + \frac{\Delta x_i}{H_k}}\right) \quad (26)$$

The effect of cascading lenses can be represented by multiplying the focusing effects of each side lens to produce a single equivalent lens, according to the scaling property of the Fourier transform. This has the effect of narrowing the beamwidth. $G_2(\theta) = G_{21}(\theta_2)$. When $M = 3$:

$$G_1(\theta) = G_{11}(\theta_{i,1})G_{12}(\theta_{i,1})G_{13}(\theta_{i,1}) \quad (27a)$$
$$G_3(\theta) = G_{31}(\theta_{i,3})G_{32}(\theta_{i,3})G_{33}(\theta_{i,3}) \quad (27b)$$

where $\theta_i = \theta + \theta_{i,k}$ and $G_{kj}(\theta)$ was defined in (25). By superposition, the lens diffraction patterns are added, so the focused EFs are given by $V_i(\theta) = \frac{1}{3}(G_1(\theta)+G_2(\theta)+G_3(\theta))$.

Assuming that pattern multiplication is valid, the final radiation pattern can be estimated as:

$$P(\theta,\theta_0) = \sum_{i=1}^{N} a_i'(\theta_0)V_i(\theta)e^{(i-1)\text{j}kd(\cos\theta-\sin\theta_0)} \quad (28)$$

where $k = \frac{2\pi}{\lambda_0}$ and d is the spacing between elements. Note that $P(\theta,\theta_0)$ dB $= 20\log_{10}|P(\theta,\theta_0)|$.

REFERENCES

[1] T. S. Rappaport, R. W. Heath Jr., R. C. Daniels, and J. N. Murdock, "Millimeter Wave Wireless Communications," Pearson Education, 2015, pp. 5, 15-16, 23-26, 319-333, 497-504, 543-548.

[2] R. C. Hansen, "Phased Array Antennas," New York: Wiley Interscience, 1998, pp. 64-67, 238.

[3] W. P. M. N. Keizer, "Synthesis of scan- and frequency-invariant low-sidelobe tapers for planar array antennas," *IEEE Trans. Antennas Propag.*, vol. 64, no. 8, pp. 3703-3707, Aug. 2016.

[4] I. A. Hemadeh, K. Satyanarayana, M. El-Hajjar and L. Hanzo, "Millimeter-wave communications: physical channel models, design considerations, antenna constructions, and link-budget," in *IEEE Comm. Surv. Tut.*, vol. 20, no. 2, pp. 870-913, 2018.

[5] M. Nickel et al., "Analysis of hybrid-passive-active phased array configurations based on an SNR approximation," in *Proc. Eur. Conf. Antennas Propag. (EuCAP)*, Paris, France, 2017, pp. 852-856.

[6] R. Wang, B. Z. Wang, X. Ding, and X. S. Yang, "Planar phased array with wide-angle scanning performance based on image theory," *IEEE Trans. Antennas Propag.*, vol. 63, no. 9, pp. 3908-3917, 2015.

[7] J. Oh, G. Z. Hutcheson, F. Aryanfar, W. Hong, and Y. J. Lee, "Planar beam steerable lens antenna system using non-uniform feed method," *IEEE Antennas Propag. Soc. AP-S Int. Symp.*, pp. 651-652, 2014.

[8] R. C. Hansen, "Microwave Scanning Antennas," Academic Press, 1966. Vol. I, p. 395, Vol. II, pp. 298-300.

[9] C. A. Balanis, "Antenna Theory: Analysis and Design," 2nd ed. Wiley, 1997, pp. 312, 371-372, 870.

[10] M. M. M. Ali and A. R. Sebak, "Design of compact millimeter wave massive MIMO dual-band (28/38 GHz) antenna array for future 5G communication systems," in *Int. Symp. Antenna Tech. Appl. Elec. (ANTEM)*, Montreal, Canada, 2016, pp. 1-2.

[11] B. Schoenlinner, X. Wu, J. P. Ebling, G. V. Eleftheriades, and G. M. Rebeiz, "Wide-scan spherical-lens antennas for automotive radars," *IEEE Trans. Microw. Theory Tech.*, vol. 50, no. 9, pp. 2166-2175, 2002.

[12] J. Ala-Laurinaho et al., "2-D beam-steerable integrated lens antenna system for 5G E-band access and backhaul," *IEEE Trans. Microw. Theory Tech.*, vol. 64, no. 7, pp. 2244-2255, July 2016.

[13] E. B. Lima, J. R. Costa, and C. A. Fernandes, "Optimization of mechanically beam-steerable lens antenna profile for 60GHz wireless communications," *IEEE Antennas Propag. Soc. AP-S Int. Symp.*, pp. 1-4, 2009.

[14] E. Gandini, A. Tamminen, A. Luukanen and N. Llombart, "Wide Field of View Inversely Magnified Dual-Lens for Near-Field Submillimeter Wavelength Imagers," *IEEE Trans. Antennas Propag.*, vol. 66, no. 2, pp. 541-549, Feb. 2018.

[15] N. T. Nguyen, A. V. Boriskin, L. Le Coq and R. Sauleau, "Improvement of the Scanning Performance of the Extended Hemispherical Integrated Lens Antenna Using a Double Lens Focusing System," *IEEE Trans. Antennas Propag.*, vol. 64, no. 8, pp. 3698-3702, Aug. 2016.

[16] E. Cagniot et al., "Cascades of π-phase plates: a transparent diffractive focusing system," *J. Opt. Soc. Am. A*, vol. 27, no. 7, pp. 1647-1654, Jul. 2010.

[17] Z. Liu, D. Zhang and J. Meng, "The Design of the Cooke Triplet Antenna in Terahertz Band," *IEEE Antennas Wirel. Propag. Lett.* vol. 18, no. 10, pp. 2199-2203, Oct. 2019.

[18] A. E. I. Lamminen et al., "Beam-switching dual-spherical lens antenna with low scan loss at 71-76 GHz," *IEEE Antennas Wirel. Propag. Lett.*, vol. 17, no. 10, pp. 1871-1875, Oct. 2018.

[19] L. Josefsson and P. Persson, "Conformal Array Antenna Theory and Design," Wiley, 2006, pp. 325-326.

[20] D. W. Boeringer and D. H. Werner, "Efficiency-constrained particle swarm optimization of a modified Bernstein polynomial for conformal array excitation amplitude synthesis," *IEEE Trans. Antennas Propag.*, vol. 53, no. 8, pp. 2662-2673, Aug. 2005.

[21] *Study of RF and EMC requirements for Active Antenna Array System (AAS) base station*, 3GPP TR 37.840 V12.1.0, 2013, pp. 79-81.

[22] H. Wheeler, "Simple relations derived from a phased-array antenna made of an infinite current sheet," *IEEE Trans. Antennas Propag.*, vol. 13, no. 4, pp. 506-514, July 1965.

[23] V. Yurlov, K. Han and N. E. Yu, "Cascaded Fresnel diffraction theorem and its application," *Opt. Engineering*, vol. 75, no. 5, Article no. 055108, pp. 1-8, 2018.

[24] Effective Focal Length Calculator, University of California San Diego. Accessed on Jul. 17, 2018. [Online]. Available: http://www-ferp.ucsd.edu/LASERLAB/TUTOR/lensdesign.shtml

[25] Y. Li and E. Wolf, "Focal Shift in Focused Truncated Gaussian Beams," *Opt. Commun.*, vol. 42, no. 3, pp. 151-156, 1982.

[26] H. D. Hristov, "Fresnel Zones in Wireless Links," Norwood, MA: Artech House Inc., 2000, pp. 51, 63-64, 180.

[27] T. A. Hill and J. R. Kelly, "28 GHz Taylor feed network for sidelobe level reduction in 5G phased array antennas," *Microw. Opt. Tech. Lett.*, vol. 61, no. 1, pp. 37-43, Jan. 2019.

[28] *White Paper on 5G Spectrum Recommendations*, 5G Americas, Apr. 2017.

[29] A. Petosa, N. Gagnon and A. Ittipiboon, "Effects of Fresnel lens thickness on aperture efficiency," in *Int. Symp. Antenna Tech. Appl. Elec. URSI Conf.*, Ottawa, Canada, 2004, pp. 1-4.

[30] M. Jiang, Z. N. Chen, Y. Zhang, W. Hong and X. Xuan, "Metamaterial-based thin planar lens antenna for spatial beamforming and multibeam massive MIMO," *IEEE Trans. Antennas Propag.*, vol. 65, no. 2, pp. 464-472, Feb. 2017.

[31] A. Abbaspour-Tamijani, K. Sarabandi and G. M. Rebeiz, "A millimetre-wave bandpass filter-lens array," *IET Microw., Antennas & Propag.*, vol. 1, no. 2, pp. 388-395, Apr. 2007.

[32] D. M. Pozar, "Microwave Engineering," 3rd ed. Wiley, 2005, pp. 64-98.

[33] J. Urbonas, K. Kim, F. Vanaverbeke and P. H. Aaen, "An Electro-Optic Pulsed NVNA Load-Pull System for Distributed *E*-Field Measurements," in *IEEE Trans. Microw. Theory and Tech.*, vol. 66, no. 6, pp. 2896-2903, June 2018.

[34] F. Foglia Manzillo et al., "A Wide-Angle Scanning Switched-Beam Antenna System in LTCC Technology With High Beam Crossing Levels for V-Band Communications," *IEEE Trans. Antennas Propag.*, vol. 67, no. 1, pp. 541-553, Jan. 2019.

[35] M. Khalily, R. Tafazolli, P. Xiao, and A. A. Kishk, "Broadband mm-wave microstrip array antenna with improved radiation characteristics for different 5G applications," *IEEE Trans. Antennas Propag.*, vol. 66, no. 9, pp. 4641-4647, Sept. 2018.

[36] E. Hecht, "Optics," 3rd ed. Addison Wesley Longman, Inc., 1998, pp. 156-159, 170, 224-225, 258-260, 459-497, 515-517.

[37] H. Markovich, D. Filonov, I. Shishkin and P. Ginzburg, "Bifocal Fresnel lens based on the polarization-sensitive metasurface," *IEEE Trans. Antennas Propag.*, vol. 66, no. 5, pp. 2650-2654, May 2018.

[38] Y. Cheng, X. Ding, W. Shao, M. Yu and B. Wang, "2-D Planar Wide-Angle Scanning-Phased Array Based on Wide-Beam Elements," *IEEE Antennas Wirel. Propag. Lett.*, vol. 16, pp. 876-879, Sept. 2016.

[39] A. Abbaspour-Tamijani, L. Zhang, and H. Pan, "Enhancing the directivity of phased array antennas using lens-arrays," *Prog. Electromagn. Res.*, vol. 29, pp. 41-64, Feb. 2013.

[40] T. A. Hill, J. R. Kelly, M. Khalily, T. W. C. Brown, "Conformal Transmitarray for Scan Loss Mitigation with Thinned Reconfiguration," in *Proc. Eur. Conf. Antennas Propag. (EuCAP)*, Krakow, Poland, 2019.

[41] T. Tuovinen, N. Tervo, and A. Parssinen, "Analyzing 5G RF System Performance and Relation to Link Budget for Directive MIMO," *IEEE Trans. Antennas Propag.*, vol. 65, no. 12, pp. 6636-6645, Dec. 2017.

[42] S. Verdù, "Spectral efficiency in the wideband regime," *IEEE Trans. Inf. Theory*, vol. 48, no. 6, pp. 1319-1343, June 2002.

[43] D. F. DiFonzo, "Satellite and Aerospace" in *The Electrical Engineering Handbook*," vol. 74, R. C. Dorf, Ed., Boca Raton, FL: CRC Press LLC, 2000.

[44] X. Ding, B. Z. Wang and G. Q. He, "Research on a millimeter-wave phased array with wide-angle scanning performance," *IEEE Trans. Antennas Propag.*, vol. 61, no. 10, pp. 5319-5324, Oct. 2013.

[45] B. Xiao, "Equivalent field of paraxial diffraction of a zone plate," *Opt. Lett.*, vol. 19, no. 23, pp. 1940-1942, 1994.
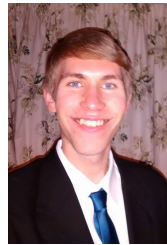
Timothy A. Hill received the MEng degree in electronic engineering from the University of Surrey in 2016. He received the Ph.D. degree in electronic engineering at the University of Surrey in 2020, specializing in millimeter wave beam steerable antennas.

In the summer of 2012, he worked at Imagination Technologies. From 2013 to 2014, he was an Engineering Intern at Qualcomm, Farnborough, developing near-field communications, power amplifier envelope tracking, and GSM RF drivers software. His research interests include millimeter wave lens and array antennas.

Dr Hill is a member of EurAAP and COST. In 2015, he was the recipient of the DTI award for Best Undergraduate RF Project, in which he developed a novel modulation scheme for 5G communications.

James R. Kelly (M'10) received the Master's degree in electronic and electrical engineering and the Ph.D. degree in microwave filters from Loughborough University, U.K., in 2002 and 2007, respectively.

From 2007 to 2012 he worked as a research fellow/associate at Loughborough University, as well as the Universities of Birmingham, Durham, and Sheffield. From 2012 to 2013 he was a Lecturer at Anglia Ruskin University, Cambridge, U.K.. In 2013 he joined the Institute for Communication Systems (ICS) at the University of Surrey, U.K.. In 2018 he joined Queen Mary University of London, where he is employed as a Lecturer in Microwave Antennas.

Dr Kelly has published over 100 academic papers in peer-reviewed journals and conference proceedings. He holds a European patent on reconfigurable antennas. He is a member of the Institution of Engineering and Technology (IET), the Institute of Electrical and Electronics Engineers (IEEE), and the IEEE Industrial Electronics Society. His primary research focus is reconfigurable antennas.

Mohsen Khalily (M'13, SM'18) is a Lecturer in Antenna and Propagation with the Institute for Communication Systems (ICS), Home of the 5G Innovation Centre (5GIC), University of Surrey, U.K., where he was a Research Fellow on antennas and propagation from December 2015 to March 2019. Prior to joining the 5GIC he was a Senior Lecturer with the Wireless Communication Centre (WCC), University Technology Malaysia (UTM). He is a Fellow of the U.K. Higher Education Academy and an IEEE Senior Member.

He has published almost 100 academic papers in international peer-reviewed journals and conference proceedings. His research interests include Large Intelligent Surface, 5G system, dielectric resonator antennas, MIMO antennas, phased arrays, circularly polarized antennas for satellite application, hybrid beam-forming, leaky wave antennas, and mm-Wave & terahertz antennas and propagation. He is also a member of the IEEE Antennas and Propagation Society, the IEEE Communication Society, and the IEEE Microwave Theory and Techniques Society; and an Associate Editor of the IEEE Access.

Tim W. C. Brown (S'00, M'04) received the B.Eng. degree in electronic engineering from the University of Surrey, Guildford, U.K., in 1999, and the Ph.D. degree in antenna diversity for mobile terminals from the Centre for Communication Systems Research (now named the Institute for Communications Systems), Guildford, U.K., in 2004. From 2004 to 2006, he was Post-Doctoral Researcher with Aalborg University, Aalborg, Denmark, where he was involved in antennas, propagation and radio frequency (RF) engineering. He is currently an Associate Professor of RF, antennas and propagation with the University of Surrey. His current research interests include intelligent antennas for mobile and satellite communications, propagation modeling from a few megahertz to tens of gigahertz, multiple-input multiple-output, ultra-wideband, and smart RF identification.